ACCEPTED MANUSCRIPT
This is the author's peer reviewed, accepted manuscript. However, the online version of record will be different from this version once it has been copyedited and typeset.
PLEASE CITE THIS ARTICLE AS DOI: 10.1063/5.0185405
Journal of Applied Physics
AIP Publishing

Reliable measurement of the density of states including occupied in-gap states of an amorphous In–Ga–Zn–O thin film via photoemission spectroscopies: Direct observation of light-induced in-gap states

Ryotaro Nakazawa,[1, a)] Atsushi Matsuzaki,[1] Kohei Shimizu,[1] Ikuko Nakamura,[2] Emi Kawashima,[2] Seiji Makita,[3] Kiyohisa Tanaka,[3] Satoshi Yasuno,[4] Haruki Sato,[1] Hiroyuki Yoshida,[1] Mojtaba Abdi-Jalebi,[5] Samuel D. Stranks,[6, 7] Syohei Tadano,[1] Peter Krüger,[1] Yuya Tanaka,[8] Hiroshi Tokairin,[2] and Hisao Ishii[1, 9, 10]

[1)] *Graduate School of Science and Engineering, Chiba University, Chiba 263-8522, Japan*
[2)] *Idemitsu Kosan Co. Ltd., Sodegaura 299-0293, Japan*
[3)] *UVSOR Facility, Institute for Molecular Science, Okazaki 444-8585, Japan*
[4)] *SPring-8 Beamline Station, National Institute for Materials Science, Hyogo 679-5198, Japan*
[5)] *Institute for Materials Discovery, University College London, London WC1E 7JE, United Kingdom*
[6)] *Cavendish Laboratory, University of Cambridge, Cambridge CB3 0HE, United Kingdom*
[7)] *Department of Chemical Engineering and Biotechnology, University of Cambridge, Cambridge CB3 0AS, United Kingdom*
[8)] *Graduate School of Science and Technology, Gunma University, Gunma 376-8515, Japan*
[9)] *Center for Frontier Science, Chiba University, Chiba 263-8522, Japan*
[10)] *Molecular Chirality Research Center, Chiba University, Chiba 263-8522, Japan*

(Dated: 24 January 2024)

Illumination stress (IS) and negative bias under illumination stress (NBIS) cause considerable device instability in thin-film transistors based on amorphous In–Ga–Zn–O (a-IGZO). Models using in-gap states are suggested to explain device instability. Therefore, to provide reliably their density of states (DOS), this study investigated the valence band, conduction band, and in-gap states of an a-IGZO thin film. The DOS of in-gap states was directly determined in a dynamic range of six orders of magnitude through constant final state yield spectroscopy (CFS-YS) using low-energy and low-flux photons. Furthermore, light irradiation irreversibly induced extra in-gap states near the Fermi level and shifted the Fermi level to the vacuum level side, which should be related to the device instability due to IS and NBIS. Hard X-ray photoemission spectroscopy and ultraviolet photoemission spectroscopy using synchrotron radiation observed the large DOS of in-gap states near the Fermi level as in previous works. Here, we reveal that they are not intrinsic electronic states of undamaged a-IGZO, but induced by the intense measurement light of synchrotron radiation. This study demonstrates that CFS-YS is useful for determining the reliable DOS of the in-gap states for samples that are sensitive to light irradiation. The absorption spectrum measured through photothermal deflection spectroscopy is interpreted based on DOS directly determined via photoemission spectroscopies. This indicates that the lineshape in the energy region below the region assigned to the Urbach tail in previous works actually roughly reflects the DOS of occupied in-gap states.

I. INTRODUCTION

Transparent amorphous oxide semiconductors exhibit excellent potential for use as materials for transparent electronic devices. In particular, amorphous In–Ga–Zn–O_4 (a-IGZO) is preferred in thin-film transistors (TFTs) in flat-panel displays over conventional amorphous Si-based TFTs. However, a-IGZO TFTs exhibit stability issues due to bias stress and illumination stress (IS). Specifically, IS and negative bias under illumination stress (NBIS) causes the transfer curve of TFTs to shift to the lower voltage side[1–5], which is irreversible[1,4] and requires annealing for recovering the performance[1].

Several models have been proposed for understanding the instabilities due to IS and/or NBIS. In the hole-trap model[3,6–8], holes generated by light irradiation drift to the interface between channel and insulator by negative bias and they are trapped in the occupied in-gap states. In the oxygen vacancy ionization model (OVI)[1–3,6,9–13], oxygen vacancies (V_O), which are the occupied in-gap states, are ionized by light irradiation to induce metastable donor states ($V_O^0 \rightarrow V_O^{2+} + 2e^-$). In the metastable peroxide defect model[9,12,14–17], holes produced by light irradiation react with the occupied in-gap states. Along with the O–O bond formation, peroxide defect ($(O–O)^{2-}$) provides electrons to the conduction band (CB) acting as the metastable state ($O^{2-} + O^{2-} + 2h^+ + 2e^- \rightarrow (O–O)^{2-} + 2e^-$). NBIS mechanism is yet to be detailed comprehensively. The occupied in-gap states and metastable states are critical for understanding the device instability mechanism due to NBIS.

Although numerous studies have focused on evaluating in-gap states[18,19], directly evaluating the DOS of in-gap states experimentally is not easy. Typically, the DOS of in-gap states is deduced through electric measurements[5,9,11,17,20–34]. However, electric measurements are indirect methods because the DOS curve is obtained by assuming some models to analyze electrical characteristics.

Optical absorption measurement is also used to evaluate the

[a)] Author to whom correspondence should be addressed: r.nakazawa19@chiba-u.jp

AIP Publishing
Journal of Applied Physics
ACCEPTED MANUSCRIPT
This is the author's peer reviewed, accepted manuscript. However, the online version of record will be different from this version once it has been copyedited and typeset.
PLEASE CITE THIS ARTICLE AS DOI: 10.1063/5.0185405

DOS of occupied in-gap states[23,35]. An exponential decay region, so-called Urbach tail[36] ($\alpha(\mathrm{h}\nu) \propto \exp(E/E_\mathrm{u})$), typically exists below the optical absorption edge in an optical absorption spectrum. Here, Urbach energy (E_u), the slope parameter of the Urbach tail, is typically substituted for the slope parameter of the occupied tail states ($E_{0\mathrm{v}}$ of the $\mathrm{DOS}(E) \propto \exp(E/E_{0\mathrm{v}})$) under the assumption that the energy width of empty tail states is considerably smaller than that of occupied tail states[23]. In principle, the absorption coefficient (α) is expressed as follows[37,38]:

$$\alpha(\mathrm{h}\nu) \propto \mathrm{h}\nu \int |M_\mathrm{fi}|^2 D_\mathrm{i}(E) D_\mathrm{f}(E-\mathrm{h}\nu) dE. \qquad (1)$$

Here, $|M_\mathrm{fi}|^2$ is the transition matrix element from initial to final states, $|M_\mathrm{fi}|^2 = |\langle \psi_\mathrm{f} | \boldsymbol{r} | \psi_\mathrm{i} \rangle|^2$. ψ_f, ψ_i, and $\boldsymbol{r}$ are the initial wave function, the final wave function, and the position vector, respectively. D_i and D_f are the initial (occupied) and final (empty) DOS, respectively. Note that α is not proportional to D_i but the convolution of D_i and D_f (joint DOS). The Urbach region is a mixture of transitions from the valence band (VB) to empty in-gap states and occupied in-gap states to the CB. Furthermore, substituting E_u for $E_{0\mathrm{v}}$ needs the assumption that $|M_\mathrm{fi}|^2$ is constant. A first-principle calculation revealed that the DOS near valence band maximum (VBM) is mostly composed of the partial density of states (PDOS) of O states and DOS near conduction band minimum (CBM) is composed of PDOS of O and In states[39]. Because the wave functions of initial and final states differ considerably, $|M_\mathrm{fi}|^2$ can not be a constant near the optical band gap. Therefore, verifying whether E_u can be substituted for $E_{0\mathrm{v}}$ is necessary.

Although photoemission spectroscopy (PES) has been applied to observe the occupied DOS for various materials directly, the case of an a-IGZO film has some challenges. The effect of photoionization cross-section is the first challenge. Recently, hard X-ray photoemission spectroscopy (HAXPES) has been used to clarify the VB and occupied in-gap states of a-IGZO[41–47] because the bulk electronic structure including the occupied in-gap states is observed by using the synchrotron radiation (SR) light source of high photon energy for long probing depth[48]. According to the calculation from Yeh et al.[40], the photoionization cross-section of heavy metal states such as the In 5s state is considerably larger than that of O 2p state in the hard X-ray region (Tab. I). Therefore, the contribution of the O 2p state, which is the primary component of the VB, should be underestimated in HAXPES. By contrast, ultraviolet photoemission spectroscopy (UPS) can be used to detect the O 2p state because of the high photoionization cross-section in the UV region. Therefore, to elucidate electronic states, combining both methods is necessary.

Second, the excitation light in PESs may damage the a-IGZO film because a-IGZO can be easily degraded by light irradiation as the a-IGZO TFTs instabilities with NBIS and IS. Nomura *et al*. suggested that the high-energy photons by synchrotron radiation (SR) in HAXPES create large metastable states near Fermi level (E_F)[41]. These states are called near-CBM states[41]. To reveal a reliable DOS of the a-IGZO film, checking whether PES measurements such as HAXPES and UPS induce photo-degradation of a-IGZO electronic states is critical.

The methods that directly observe the changing electronic states during NBIS and/or IS have been limited. For example, Mativenga *et al.* suggested device instability due to NBIS results from metastable donors in the OVI model[1]. However, metastable donors were not directly observed by X-ray photoemission spectroscopy. Studies have discussed the correlation between TFTs characteristics and the DOS of in-gap states estimated from indirect methods[5,11,17,34]. Thus, a novel method is required to directly observe the changing DOS of in-gap states due to light irradiation.

Previously, we demonstrated high-sensitivity ultraviolet photoemission spectroscopy (HS-UPS) using low-energy photons ($\mathrm{h}\nu$ = 8.5–4 eV) to evaluate the DOS of the in-gap states of an a-IGZO thin film from the VBM to E_F in sensitivity to detect down to the 10^{14} $\mathrm{cm^{-3}eV^{-1}}$ level by connecting the HS-UPS spectra through the constant final state yield spectroscopy method (CFS-YS)[49]. CFS-YS was established by Sebastiani *et al.*[50]. Recently, CFS-YS has been applied to hydrogenated amorphous silicon[51,52], halide perovskites[53–55], and organic semiconductors[56]. Also, in principle, the probing depth of CFS-YS measuring low-energy photoelectrons is in the same order as HAXPES[48,57]. We revealed that $E_{0\mathrm{v}}$ determined by the CFS-YS spectrum differed considerably from E_u obtained by photothermal deflection spectroscopy (PDS), which indicated the importance of directly observing the DOS of in-gap states. The CFS-YS spectrum did not exhibit any special electronic states near E_F such as the near-CBM states observed by HAXPES in the literature[41,42]. It is expected that the CFS-YS can determine the DOS of occupied in-gap states without light irradiation damage because excitation photons used in the CFS-YS measurement are low-energy and low-photon flux. To clarify this phenomenon, using both methods for the same sample is necessary. Furthermore, if CFS-YS induced very small sample damage, changes in in-gap states due to light irradiation can be directly observed in CFS-YS by exposing the a-IGZO thin film to strong light irradiation that differs from that of CFS-YS.

In-gap states have been widely reported in oxides, such as ceria[58], zirconia[59], titania[60–63], SnO_2[62,64], amorphous zinc-tin-oxide[65], etc. Furthermore, device instability due to NBIS has been widely reported in TFTs based on transparent oxide semiconductors, such as Zn–O[6], amorphous In–Sn–Zn–O[12], amorphous In–W–O[66], etc. Models using in-gap states have been proposed to understand the instability of these devices, as in the case of a-IGZO. Therefore, it is important to establish a method to directly determine the DOS of in-gap states

TABLE I. Photoionization cross-section in UV and Hard X-ray photons calculated by Yeh *et al.*[40]

	Photoionization cross-section (in Mb = 10^6 barn)		
State	UV (16.7 eV)	UV (26.8 eV)	Hard x-ray (8047 eV)
O 2p	10	9.8	3.8×10^{-7}
Zn 3d		4.4	4.7×10^{-6}
Ga 4s	1.7×10^{-3}	1.2×10^{-1}	3.4×10^{-5}
In 5s	8.8×10^{-3}	1.2×10^{-1}	5.3×10^{-5}

AIP Publishing
Journal of Applied Physics
ACCEPTED MANUSCRIPT
This is the author's peer reviewed, accepted manuscript. However, the online version of record will be different from this version once it has been copyedited and typeset.
PLEASE CITE THIS ARTICLE AS DOI: 10.1063/5.0185405

without sample damage of materials that are sensitive to light irradiation. By using the method, observing the change in the DOS of in-gap states due to photo-irradiation will lead to the development of studies about oxides.

Since a-IGZO is a n-type semiconductor, the DOS of the CB is crucial to its device performance. So far, conventional inverse photoemission spectroscopy (IPES) has been performed[67]. In the literature, the major onset of the empty states was determined by linear extrapolation of an IPES spectrum. The onset energy was approximately 1.8 eV away from E_F. The tail structure visible in the IPES spectrum extended below this onset, up to E_F. This tail structure should be ascribed to the DOS of the CB edge because the CBM energy of a n-type semiconductor should be located near E_F. On the other hand, the tail may be caused by sample damage by irradiation of a high kinetic energy electron beam as well as the low energy resolution of IPES. Low-energy IPES (LEIPS) was recently developed to overcome these problems[68,69]. In this technique, the sample damage is significantly reduced by lowering the electron energy, and the energy resolution is improved by a factor of two[68,69]. Particularly, signal-to-noise ratio is markedly improved, and LEIPS is suitable to examine the DOS of the conduction band edge in this study.

In this study, we directly investigated both the occupied and empty electronic states of a-IGZO through HAXPES, HS-UPS using SR (SR-HSUPS), CFS-YS using low-energy photons with low-photon flux, and LEIPS. UPS is useful for determining the total DOS of VB because UPS mainly detects the PDOS of O states, which is the main component of VB, due to a large photoionization cross-section. In CFS-YS measurement, the DOS of occupied in-gap states was determined in a dynamic range of six orders of magnitude without sample damage. Although HAXPES and SR-HSUPS observed near-CBM states as in the previous study[41,42], they are created by intense excitation photons of SR for measurements and should not be interpreted as the intrinsic DOS. Thus, our study provides the reliable DOS landscape of the VB, CB, and occupied in-gap states of a-IGZO by integrating these PES results. Furthermore, UPS and CFS-YS measurements directly observed the reduction of the work function and the emergence of the extra in-gap states near E_F (near-CBM states) due to the intense light irradiation, respectively. The results hint that TFT instabilities due to NBIS and IS should be attributed to the change in in-gap states and the work function due to light irradiation. In addition to PES measurements, the optical absorption measurement using PDS was performed. The absorption spectrum is interpreted by joint DOS based on the DOS directly determined by PESs. This indicates that the lineshape in the energy region assigned to the Urbach tail in previous works does not reflect the DOS lineshape of occupied in-gap states. The lineshape in the energy region below the region of the Urbach tail roughly reflects it.

II. EXPERIMENTAL

DC magnetron sputtering (ULVAC; CS200) was used to deposit a-IGZO thin films (In:Ga:Zn $\sim$ 1:1:1) on Si wafer (n^+) and quartz substrate at a base pressure of 2×10^{-4} Pa. The sputtering pressure was 0.5 Pa, and the partial oxygen pressure was 10 vol.%. After deposition, the films were heat treated at 300°C for 1 h with a hot-air dryer at 23°C and 50% humidity environment to improve the electron transport. Hall mobility and carrier concentration obtained by Hall effect measurement (TOYO Corp.; ResiTest8400) at room temperature were 5 cm^{2}V^{-1}s^{-1} and 10^{14} cm^{-3}, respectively.

HS-UPS measurements using low-energy photons were performed with a home-made system at Chiba University. Here, D_2 (Hamamatsu Photonics K. K.; L1836, 150 W) and Xe lamps (Ushio Inc.; UXL-500D, 500 W) were used as light sources (hν = 8.5–3 eV). Their light was monochromatized by a zero-dispersion double monochromator (Bunkoukeiki Co., Ltd.; BIP-M25-GTM) to achieve low stray light (10^{-9} at 632 nm). By eliminating stray light, background levels were reduced to enable UPS measurements with high sensitivity. A photomultiplier tube (Hamatsu Photonics K. K.; R376, R6836) estimated the photon flux to be approximately 10^7–10^{11} cm^{-2}s^{-1}. The incidence angle of excitation light was 55° from the surface normal. A He lamp (Scienta Omicron, Inc.; HIS13) was used to perform traditional UPS measurement using HeI$_\alpha$ light (21.22 eV), which contains a few percent of HeI$_\beta$ (23.09 eV). Therefore, observing occupied in-gap states is difficult due to the shifted replica of the VB spectrum excited by the HeI$_\beta$. UPS measurements using HeI are denoted as HeI-UPS to be distinguished from HS-UPS. Photoelectrons were detected at normal emission using an electrostatic hemisphere analyzer (PSP Vacuum Technology Ltd.; RESOLVE 120). The instrumental function and E_F position were determined by using the Fermi edge of a gold film. The overall energy resolution was approximately 0.25 eV with 21.2 and 7.7 eV photons at room temperature. A sample bias voltage of -10 V was applied for all measurements to ensure that the vacuum level of the sample was higher than the vacuum level of the analyzer. The work function was determined from the secondary electron cut-off (SECO) in the HS-UPS spectrum.

In CFS-YS measurement, the analyzer measured the count of photoelectrons at a fixed kinetic energy with changing incident photon energy. The kinetic energy of measured photoelectrons was set to be 0.15 eV to correspond to the SECO peak energy of HS-UPS spectra to improve the signal-to-noise ratio. The photoelectron count was normalized by incident photon flux to obtain the external quantum efficiency of photoemission partial yield. Although photoemission partial yield was normalized by incident photon flux and absorptance in literature[52] , in this study the count of photoelectrons was not normalized absorptance because it is unknown whether all absorbed photons contribute to the photoelectron partial yield. We simulated absorbance spectra at h$\nu < 6.4$ eV by using the measured absorption spectrum in Fig. 6(a) and assuming the probing depth of CFS-YS to be 5 and 20 nm. The measured absorption and calculated absorbance spectra were monotonic functions of hν, and normalizing photoemission partial yield by absorptance had a small effect on the CFS-YS lineshape. The CFS-YS curve distribution, $N_{\text{CFS-YS}}$, can be expressed as

AIP Publishing
Journal of Applied Physics
ACCEPTED MANUSCRIPT
This is the author's peer reviewed, accepted manuscript. However, the online version of record will be different from this version once it has been copyedited and typeset.
PLEASE CITE THIS ARTICLE AS DOI: 10.1063/5.0185405

follows[49,52]:

$$N_{\text{CFS-YS}}(E) \propto \text{h}\nu |M_{\text{fi}}|^2 D_{\text{i}}(E). \quad (2)$$

In this study, the CFS-YS spectrum was normalized by hν to determine the D_{i}. If $|M_{\text{fi}}|^2$ could be measured or calculated, the CFS-YS spectrum directly reflects D_{i}. Because we have no information on $|M_{\text{fi}}|^2$, D_{i} was determined by under the assumption that $|M_{\text{fi}}|^2$ was constant. In the case of amorphous Si:H, $|M_{\text{fi}}|^2$ was proportional to $(\text{h}\nu)^{-5}$ at h$\nu > 3.4$ eV in a literature[70]. Even if $|M_{\text{fi}}|^2$ of a-IGZO was proportional to $(\text{h}\nu)^{-5}$, the intensity of the CFS-YS spectrum would only change by about one order of magnitude at maximum. So, the assumption that $|M_{\text{fi}}|^2$ was constant is not bad.

The sample was exposed to light irradiation using another Xe light source (Asahi Spectra Co., Ltd.; MAX-350) to investigate the effect of light irradiation on electronic states. The sample was exposed to light irradiation at 4.06 eV or white light irradiation (1.9–4.6 eV) by white light of the Xe lamp with or without a bandpass filter, respectively. The photon flux of the light irradiation at 4.06 eV and white light was estimated to be approximately 10^{15} cm^{-2}s^{-1} and 10^{17} cm^{-2}s^{-1} at the sample position, respectively. This strong light irradiation was denoted "light irradiation stress" to distinguish it from the excitation light of HS-UPS and CFS-YS measurements. Note that infrared radiation was eliminated to prevent sample heating during light irradiation stress. After turning off light irradiation stress, CFS-YS measurement was performed.

UPS using synchrotron radiation (SR-UPS) was performed at BL7U (SAMURAI) in UVSOR[71,72]. A Wadsworth-type monochromator was used to monochromatize SR. To measure the VB, the photon energy of the excitation light was set at 28 eV. When the photon energy of excitation light was 10.5 eV, a high-order light cut filter was inserted to achieve highly sensitive measurements to observe occupied in-gap states, which is called "SR-HSUPS". Photon flux was estimated to be approximately 10^{15} cm^{-2}s^{-1} at h$\nu = 10.5$ eV. An electrostatic hemisphere analyzer (MB Scientific AB; A-1) at normal emission was used to analyze the spectra. The energy resolution and E_{F} position were determined using the Fermi edge of a gold film at room temperature, and the overall energy resolution was approximately 0.15 eV.

HAXPES measurement was performed at BL46XU in SPring-8[73]. The incident photon energy was monochromatized at approximately 7.94 keV. The photoelectrons were detected at the take-off angle of 80° from a surface with an electrostatic hemisphere analyzer (Scienta Omicron, Inc.; R-4000 L1-10kV). The overall energy resolution was approximately 0.29 eV at room temperature.

LEIPS was measured at Chiba University[74]. In LEIPS measurement, an electron beam was incident normal to the sample surface. The emitted photon was selected by a bandpass filter with the center wavelength of 257 nm (Semrock Inc.; BrightLine series) and detected with a photomultiplier tube (Hamamatsu Photonics K.K.; R585s). We carefully examined the optimal sample current. When the current increased to 500 nA, we observed large changes in the lineshape of LEIPS and low-energy electron transmittance (LEET) spectrum which shifted approximately 0.5 eV to the high energy side. When the current was less than 80 nA, the LEIPS spectrum did not change, and the LEET spectrum was shifted by only 0.05 eV. Thus, we performed LEIPS measurements at 80 nA throughout this work. The energy resolution and E_{F} position were determined by the Fermi edge of a polycrystalline silver film at room temperature. The energy resolution was approximately 0.45 eV, roughly 2–3 times broader than that of HAXPES, SR-(HS)UPS, HeI-UPS, and HS-UPS. To estimate the "true" DOS, the observed spectrum was deconvoluted with the instrumental function through the iterative nonlinear deconvolution method[75].

The PDS measurement was performed at University of Cambridge. The 50-nm-thick a-IGZO film was prepared on a quartz substrate as the sample. Photon absorption by the sample was detected as a refractive index gradient in the area surrounding the sample surface. By immersing the sample in an inert liquid FC-72 Fluorinert (3M Company) with a high refractive index change due to temperature, photoabsorption can be detected with high-sensitivity. The details were described in a previous study[76].

III. RESULTS AND DISCUSSION

A. Valence band electronic states

Figure 1 displays the VB electronic states measured through HAXPES, SR-UPS, HeI-UPS, and CFS-YS. The horizontal axis is the electron binding energy relative to the Fermi level (E_{B}^{F}). In HAXPES, VBM energy is determined to be at E_{B}^{F} =3.25 eV by linear extrapolation of the spectrum onset. The spectrum peaks at approximately 9 and 11 eV. VBM energy and lineshape are consistent with previous studies[41,42,77].

In the SR-UPS, the linear extrapolation of the spectrum onset revealed that the VBM energy was at $E_{\text{B}}^{\text{F}} = 3.69$ eV. This value is overestimated due to the sample damage of incident excitation photons of SR, which will be described in Sec. III E. The SR-UPS spectrum has a long tail at $E_{\text{B}}^{\text{F}} < 4$ eV. This tail is not a real electronic state and results from a higher-order light. The SR-UPS spectrum differs considerably from the HAXPES spectrum: the lineshape peaks at approximately 5 and 11 eV.

We compare the lineshapes among HAXPES, SR-UPS, and the calculation in the literature[39]. Considering the photoionization cross-section (Tab. I), in the SR-UPS spectrum (hν = 28 eV), the peaks at approximately 5 and 11 eV can be assigned as the PDOS of O and Zn states, respectively. Because they are the primary component of the VB, the SR-HSUPS spectrum is consistent with the total DOS. On the other hand, the HAXPES spectrum (hν = 7.94 keV) does not peak at $E_{\text{B}}^{\text{F}} = 3$–6 eV because (i) the PDOS of O states is the primary component of the peak of total DOS in the VB top region and (ii) the HAXPES excitation cross-section of O is much lower than for the other elements. The peak of the HAXPES at approximately $E_{\text{B}}^{\text{F}} = 9$ eV is attributed to the PDOS of In and Ga states, and the peak of the HAXPES at approximately $E_{\text{B}}^{\text{F}} = 11$ eV is ascribed to the PDOS of Zn states. Although the previ-

ACCEPTED MANUSCRIPT
Journal of Applied Physics
AIP Publishing
This is the author's peer reviewed, accepted manuscript. However, the online version of record will be different from this version once it has been copyedited and typeset.
PLEASE CITE THIS ARTICLE AS DOI: 10.1063/5.0185405

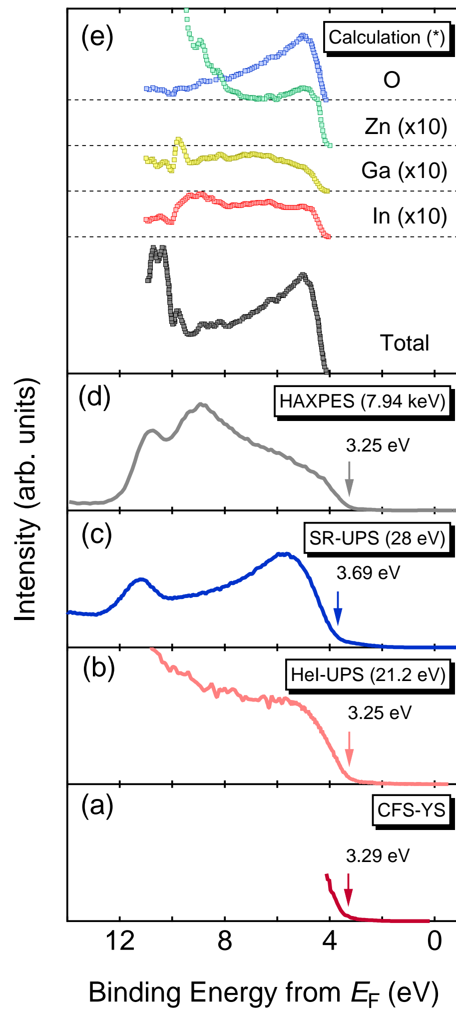

FIG. 1. Valence band (VB) electronic states measured through (a) constant final state yield spectroscopy (CFS-YS, hν < 8.5 eV), (b) ultraviolet photoemission spectroscopy using HeI (HeI-UPS, hν = 21.2 eV), (c) UPS using synchrotron radiation (SR-UPS, hν = 28 eV), (d) hard X-ray photoemission spectroscopy (HAXPES, hν = 7.94 keV), and (e) Calculated total density of state (DOS) and partial DOS (PDOS) in the literature(*)[39]. Fermi level (E_F) is set to 0.0 eV.

ous study ascribed the region at $E_B^F = 3$–10 eV to hybridized O states[41], the HAXPES from 3 to 10 eV should be derived from PDOS of In and Ga states.

The spectral intensity of HeI-UPS (hν = 21.22 eV) increases considerably from 3 eV toward deeper E_B^F with the gradual increase in the background. The HeI-UPS clearly observes the VB top region ascribed to the PDOS of O states. The VBM energy is determined to be at $E_B^F = 3.25$ eV by the linear extrapolation of HeI-UPS onset.

In the CFS-YS measurement, because the excitation photon energy was limited at hν < 8.5 eV, CFS-YS reveals only DOS around the VB onset region.

B. Conduction band electronic states

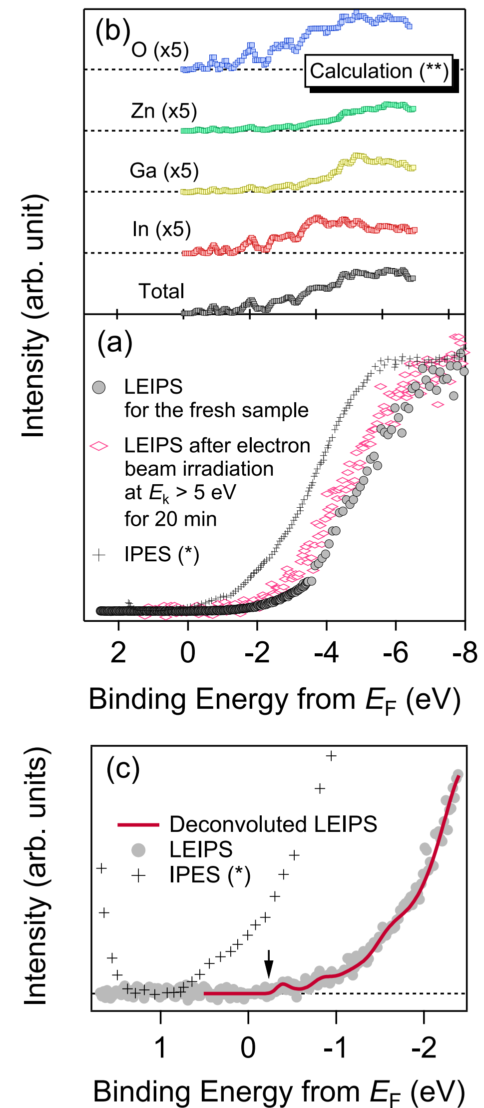

FIG. 2. (a) Conduction band (CB) electronic state measured through low-energy inverse photoemission spectroscopy (LEIPS) and conventional inverse photoemission spectroscopy (IPES) in the literature (*)[67]. E_F set to 0.0 eV. (b) Calculated total DOS and PDOS in the literature(**)[39]. (c) Expanded figure near E_F. The red line denotes the deconvoluted LEIPS spectrum.

Figure 2(a) displays the CB electronic states measured through LEIPS. The horizontal axis is binding energy relative to E_F. LEIPS spectral intensity gradually increases in the negative E_B^F region (the region of empty states). The LEIPS intensity near CBM is small, which agrees with the calculated total DOS in the literature[39] shown as Fig. 2(b). The IPES spectrum in the literature[67] is shifted from the LEIPS spectrum by around 1 eV. The energy shift of the IPES spectrum should be due to the sample damage of the electron beam. The difference between the IPES and LEIPS measurement is

ACCEPTED MANUSCRIPT
Journal of Applied Physics
AIP Publishing
This is the author's peer reviewed, accepted manuscript. However, the online version of record will be different from this version once it has been copyedited and typeset.
PLEASE CITE THIS ARTICLE AS DOI: 10.1063/5.0185405

the energy of the detected photon: IPES and LEIPS detect photons at h$\nu \sim 9$ eV and h$\nu = 4.82$ eV, respectively. The work function is determined to be 4.2 eV by LEET measurements in LEIPS. Thus, the IPES in the literature requires the electron beam with $E_k > 4.8$ eV to examine the empty electronic states. On the other hand, LEIPS needs the electron beam with $E_k > 0.6$ eV. Therefore, in principle, LEIPS can evaluate CB electronic states by minimizing sample damage. To support this, we performed the LEIPS measurement after electron beam irradiation at $E_k = 5$–10 eV for 20 min with the current at ~80 nA. In Fig. 2(a), the LEIPS spectrum after electron beam irradiation shows a shift to the E_F, indicating that the electronic states during the IPES should not be free from the sample damage by the electron beam.

To determine the CBM energy by LEIPS spectrum, the expanded figure near the E_F is displayed as Fig. 2(c). CBM energy is determined to be at $E_B^F = -0.26$ eV by linear extrapolation of the LEIPS spectrum onset. We can believe that the CBM energy obtained through LEIPS is reasonable compared with that determined by IPES in the literature[67] with a big tail extending to around E_F due to the sample damage and low-energy resolution. Deconvolution was supplementally performed to confirm the CBM energy of the LEIPS spectrum. The onset energy of the deconvoluted LEIPS spectrum is approximately −0.2 eV, supporting the validity of the CBM energy obtained from the linear extrapolation of the LEIPS spectrum, $E_B^F = -0.26$ eV. Note that a higher signal-to-noise ratio is required to discuss the electronic states of CB in more detail by using the LEIPS and deconvoluted LEIPS spectrum.

Next, the LEIPS spectrum is compared with the calculated DOS. The calculated DOS was shifted so that their onset energies aligned with the experimental spectrum. The onset region of the total DOS consists of the PDOS of O and In states. We assume the LEIPS cross-section is proportional to that of the photoionization[78]. Because the photoionization cross-section data in the energy detected in the LEIPS measurements (hν = 4.82 eV) is not available, we assumed the photoionization cross-sections among the elements are similar to those at hν = 16.7 eV (Tab. I). If this is the case, the LEIPS spectrum should show the PDOS of O states about 1000 times stronger than that of In. Thus, we can assign the LEIPS onset structure to the PDOS of O states.

C. Occupied in-gap states

Figure 3(a) shows occupied in-gap states obtained through HAXPES. The upper and bottom figures are in linear and log scales, respectively. The background level was subtracted for the HAXPES spectrum to make intensity from −0.5 to −1 eV (empty states region) zero. Two in-gap states were observed. One is widely distributed with high intensity near VBM (3–1.5 eV), so-called near-VBM states. Tail states are not observed because near-VBM states with high intensity bury them. The lineshape of near-VBM states is in line with previous findings on a film with similar Hall mobility and electron concentration[77] and high-quality films with Hall mobility at 2–3 times higher than our sample[42,77] in the previous

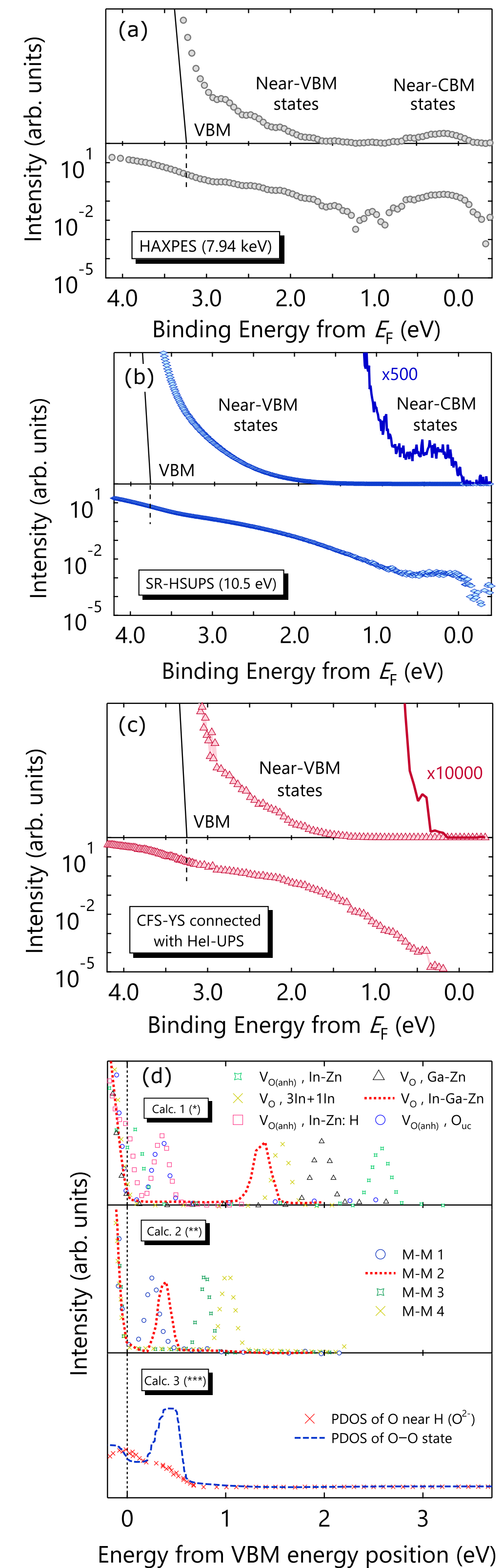

FIG. 3. Occupied in-gap states obtained through (a) HAXPES, (b) SR-HSUPS, and (c) CFS-YS connected with HeI-UPS. Upper and bottom figures are linear and log scale, respectively. (d) Calculated in-gaps states in literature(*)[79], (**)[16], and (***)[80]. The zero set at VBM energy position.

AIP Publishing
Journal of Applied Physics
ACCEPTED MANUSCRIPT
This is the author's peer reviewed, accepted manuscript. However, the online version of record will be different from this version once it has been copyedited and typeset.
PLEASE CITE THIS ARTICLE AS DOI: 10.1063/5.0185405

works. The other is localized near E_F (from 1 to -0.2 eV), so-called the near-CBM states.

Figures 3 (b) and (c) reveal SR-HSUPS and CFS-YS overlapped with the HeI-UPS spectrum, respectively. The background level was subtracted for the SR-HSUPS to make intensity from -0.5 to -1 eV (empty states region) zero. Near-VBM states are observed through SR-HSUPS and CFS-YS as well as the HAXPES.

The spectra lineshape and intensity of Near-CBM states are different among HAXPES, SR-HSUPS, and CFS-YS. In HAXPES, near-CBM states are observed as a peak shape. The near-CBM states intensity of the SR-HSUPS is less than that of HAXPES. In the CFS-YS measurements, the near-CBM states completely disappear. The origin of near-VBM and CBM states will be discussed in III E.

D. Effect of light irradiation on electronic states

We examined the effect of light irradiation on the electronic states of the a-IGZO through CFS-YS measurements because IS and NBIS cause considerable device instability in TFTs based on a-IGZO. The CFS-YS spectrum depicted as red triangles in Fig. 4 (a) is the first scan for the fresh sample. The horizontal axis is binding energy from the vacuum level (E_B^V). In Fig. 4(a), the E_F position was determined by the work function. The E_F positions are indicated as the arrows in the same color as the CFS-YS spectra.

After the first scan CFS-YS, the E_F position shifts from 4.32 (red arrow) to 4.23 eV (pink arrow). Therefore, CFS-YS was performed again to check the changing distribution of in-gap states. The intensity of the second scan CFS-YS increases in the near E_F region ($E_B^V = 4.8$–4 eV) without any change in the near-VBM region ($E_B^V = 8$–5 eV). The newly created electronic states due to light irradiation are called "extra in-gap states" in this article. The intensity of extra in-gap states at the third scan increases more than that at the second scan, but the E_F position does not change. After the third scan, the CFS-YS lineshape and the E_F position do not change.

Next, the sample was exposed to light irradiation stress at $h\nu = 4.06$ eV for 50 min using another Xe light source through the bandpass filter. The photon flux of this light irradiation stress was estimated to be around 10^{15} cm^{-2}s^{-1}, which is approximately more than 1000 times higher than that of the excitation light during CFS-YS and HS-UPS measurements. The kinetic energy distribution of photoelectrons during light irradiation stress at $h\nu = 4.06$ eV was measured. Fig. 4(b) displays the observed UPS spectra averaged every 5 min, and Fig. 4(c) plots the work function and the UPS intensity at the peak as a function of the light irradiation time. During light irradiation stress at $h\nu = 4.06$ eV, the work function changes from 4.23 to 4.0 eV, and the peak intensity increases by approximately 25 times. UPS results reveal that the change in electronic states depends on the light irradiation time. After the light irradiation stress at $h\nu = 4.06$ eV was turned off, CFS-YS was then performed. The CFS-YS detects extra in-gap states in the region at $E_B^V > 3.7$ eV. The E_F position is $E_B^V = 4.0$ eV (yellow arrow) and the CFS-YS intensity of ex-

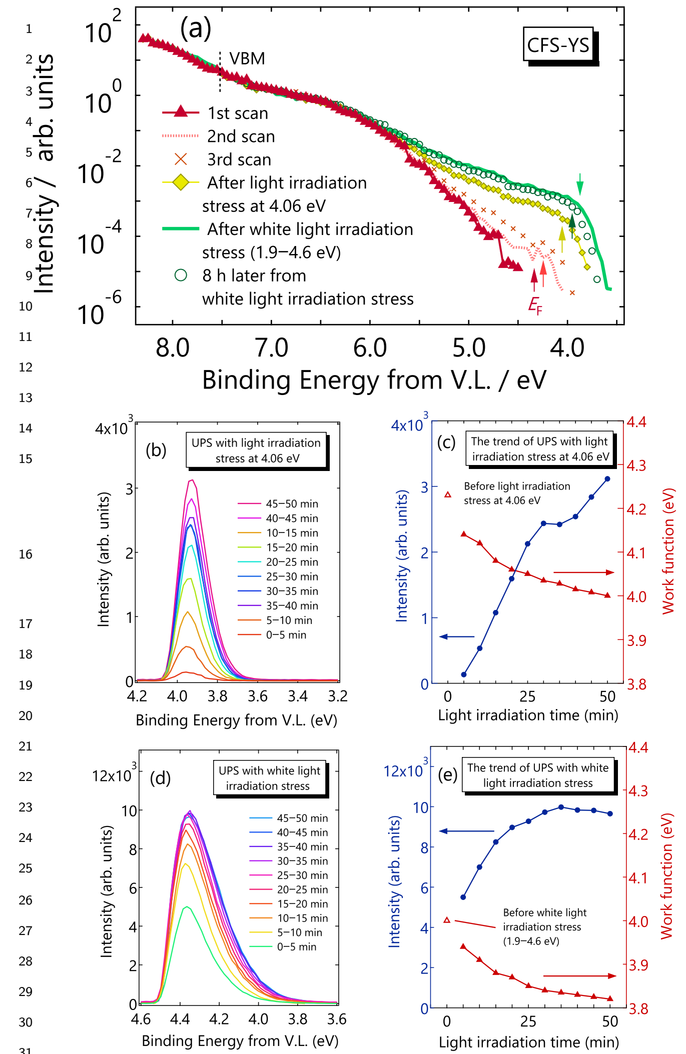

FIG. 4. (a) Change in the electronic states due to light irradiation observed by CFS-YS measurements. The horizontal axis is the binding energy from the vacuum level. E_F position is indicated as the arrow in the same color as the CFS-YS spectrum. (b) UPS spectra during the light irradiation stress at $h\nu = 4.06$ eV for 50 min. (c) The trends of peak intensity and work function in (b). (d) UPS spectra during the white light irradiation stress ($h\nu = 1.9$–4.6 eV) for 50 min. (e) The trends of peak intensity and work function in (d).

tra in-gap states at $E_B^V = 3.9$ eV is approximately 25 times as much as that before light irradiation stress, which is quantitatively consistent with the change of the UPS spectra in Fig 4(c).

The sample was exposed to white light irradiation stress without any bandpass filters to accelerate photo-degradation. The light included photons at $h\nu = 1.9$–4.6 eV. Photon flux was estimated to be approximately 10^{17} cm^{-2}s^{-1}. Fig. 4(d) displays UPS spectra averaged every 5 min during white light irradiation stress. Because white light contains photons at $h\nu = 1.9$–4.6 eV, UPS spectra during white light irradiation stress broaden more than that during light irradiation stress at $h\nu = 4.06$ eV. Fig. 4(e) shows the plot of UPS intensity at the peak and work function during white light irradiation stress as

Journal of Applied Physics
ACCEPTED MANUSCRIPT
AIP Publishing
This is the author's peer reviewed, accepted manuscript. However, the online version of record will be different from this version once it has been copyedited and typeset.
PLEASE CITE THIS ARTICLE AS DOI: 10.1063/5.0185405

a function of irradiation time. The peak intensity is saturated for approximately 35 min. The work function decreases from 4.0 to 3.87 eV. After the white light irradiation, the E_F position is at $E_B^V = 3.87$ eV (green arrow) and the CFS-YS intensity of extra in-gap states at $E_B^V = 4.3$ eV increases two times as much as that before white light irradiation, corresponding to the change of the UPS spectra in Fig. 4(e).

Extra in-gap states produced by light irradiation stress do not exhibit any change after 8 h from white light irradiation stress and the E_F position remains at $E_B^V = 3.93$ eV, indicating that these changes in electronic states due to light irradiation stress are irreversible. The origin of these changes due to light irradiation stress will be discussed in the next section.

E. Landscape of electronic states

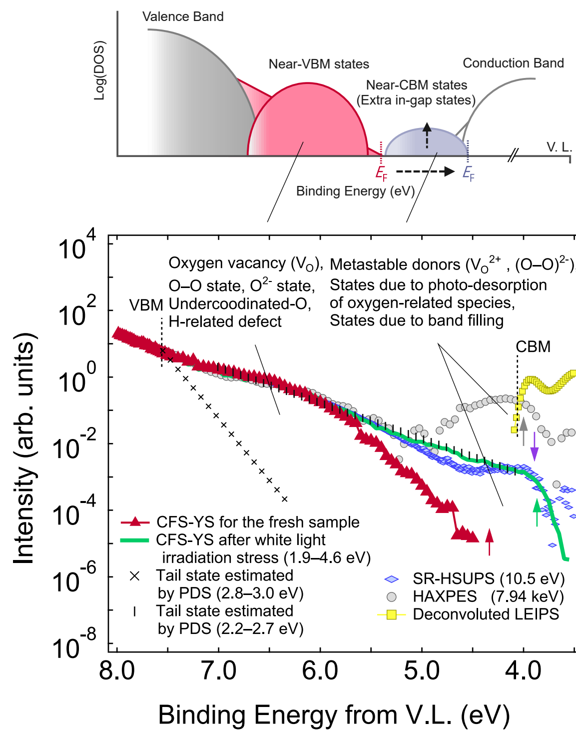

FIG. 5. Landscape of the electronic states of the VB, in-gap states, and the CB determined by the CFS-YS, HAXPES, SR-HSUPS, and deconvoluted LEIPS in the log scale. Here, the E_F is indicated as the arrow in the same color as the spectrum. CFS-YS observes the DOS of in-gap states without sample damage due to light irradiation. Occupied in-gap states, which are estimated by traditional Urbach energy of photothermal deflection spectroscopy (PDS) at hν = 2.8–3 eV, differs from PES results. DOS of occupied in-gap states, which are estimated by PDS at hν = 2.2–2.7 eV, is roughly consistent with SR-HSUPS and CFS-YS after white light irradiation stress.

In this section, by comparing the results of LEIPS, HAXPES, SR-HSUPS, and CFS-YS, we will provide a reliable DOS landscape of in-gap states including the VB and CB edges. The origin of the in-gap states will be discussed. Then, we will comment on the advantages and disadvantages of each PES technique.

Figure 5 displays the DOS landscape of a-IGZO in log scale. Because we reveals in Sec. III D that light irradiation stress results in shifting E_F to the vacuum level side, the horizontal axis is the binding energy from the vacuum level (E_B^V) to eliminate the shift of E_F due to light irradiation of each measurement. The SR-HSUPS (hν = 10.5 eV) was connected with the SR-UPS (hν = 28 eV) by overlapping around the VBM region. CFS-YS spectra, performed on the fresh sample and the sample after white light irradiation stress, are plotted. The energy positions of HAXPES and SR-HSUPS were calibrated to ensure that their VB region matches the HeI-UPS. Their intensities were normalized in the VB. The ionization potential is determined to be 7.55 eV by the HeI-UPS spectrum onset in linear scale, which is in the range of the reported value from 7.2 to 8.25 eV[45,81,82].

Focusing on the region of $E_B^V > 5.5$ eV, CFS-YS, SR-HSUPS, and HAXPES observes near-VBM states. From the comparison of PES results and theoretical calculations, we discuss the origin of the near-VBM states. Fig. 3 (d) displays the results in reported calculations[16,79,83]. The VBM energy position is set at 0.0 eV.

A possible origin of near-VBM states is oxygen vacancies (V_O). In calculation 1 by Köener *et al.*[79], oxygen-lacking samples were obtained by removing a single O atom from each equilibrated stoichiometric amorphous supercell, resulting in a metal−metal defects (M–M defects). This is characterized by a metal atom and its adjacent atoms which are directly connected without any oxygen bonds. In–Zn, Ga–Zn, In–Ga–Zn, and 3In+1In defects are widely distributed as occupied in-gap states of V_O for each sample. In calculation 2 by Meux *et al.*[16], M–M defects form occupied in-gap state in the lower band gap for each calculated model, which was obtained by removing (or strongly displacing) an oxygen atom from stoichiometric atomic models. Other calculations[83,84] agreed that V_O is the origin of occupied in-gap states, which is located around 1 eV from the VBM energy position.

Besides V_O, other origins of occupied in-gap states have been reported in literature. In calculation 3 by Robertson *et al.*[80], in the case of adding one interstitial O into a supersell of a-IGZO, the PDOS of peroxide defect (O–O state) provides a defect state in the gap just above the VBM. In the case of adding one interstitial O and two H close to this O, O^{2-} gave defect states near VBM. Calculation 1 by Köener *et al.*[79] argued that the In-Zn defects decrease energy with H doping, and the occupied in-gap states near VBM due to H is visible. Some literature[84,85] revealed that hydrogen bonds with other elements become an occupied in-gap state near VBM. Calculation 1 also suggested that the occupied in-gap state approximately 0.5 eV away from VBM is attributed to undercoodinated-O.

Judging from the energy width and position, near-VBM states observed by PESs cannot be identified as the specific origin as mentioned, V_O, undercoodinated-O, O–O state, O^{2-} state, and H-related defect. The energy width of near-VBM states observed by PESs is clearly broader than that of in-gap states obtained by theoretical calculations. This discrepancy

ACCEPTED MANUSCRIPT
Journal of Applied Physics
AIP Publishing
This is the author's peer reviewed, accepted manuscript. However, the online version of record will be different from this version once it has been copyedited and typeset.
PLEASE CITE THIS ARTICLE AS DOI: 10.1063/5.0185405

must result from statistical differences. The theoretical calculations use a supercell missing or adding several atoms although a realistic a-IGZO thin film contains many types of defects. Therefore, in-gap states observed by PESs are expected to be statistically averaged. Besides, calculation 1 revealed that the energy positions of Ga–Zn defect differ by more than 0.5 eV for each sample, indicating that the energy position of a defect level is not only determined by the species and number of metal atoms directly involved but also by the whole local arrangement around missing oxygen atoms[79]. Extending the size of a supercell and containing more defects are required to compare near-VBM states observed by PESs with calculations.

Focusing on the region of $E_B^V < 5.5$ eV, PES lineshapes differ for each measurement. Near-CBM states are observed by SR-HSUPS and HAXPES measurements, whereas CFS-YS do not observe them. In SR-HSUPS and HAXPES, photoelectrons are observed even below the E_F for the fresh sample ($E_B^V < 4.32$ eV). After white light irradiation stress in the photo-degradation experiments in Fig. 4, The E_F position is shifted from 4.32 eV (red arrow) to 3.87 eV (green arrow), which is around the E_F in the SR-HSUPS (blue arrow) and HAXPES spectra (grey arrow). The CFS-YS lineshape after white light irradiation stress resembles the SR-HSUPS lineshape due to the creation of the extra in-gap states.

Here, let us discuss the origin of the changing of electronic states due to light irradiation stress in CFS-YS measurements in Fig. 4. The OVI model can be one of the explanations for this change of electronic states due to light irradiation stress. Previous studies suggested that when V_O is ionized to V_O^{2+}, the atoms around V_O relax considerably to result in metastable shallow donors[86,87]. Noh *et al.* performed molecular dynamics simulations within the first principle calculation for the structural relaxation when V_O^{2+} captures two electrons[87]. They revealed that V_O^{2+} defects do not return to V_O defects even at annealing temperatures of 500–600°C, becoming shallow donors. In our case, the photon energy of light irradiation stress ($h\nu = 4.06$ eV or 1.9–4.6 eV) is sufficient to ionize V_O to V_O^{2+} due to the transition from V_O to the CB. In addition, extra in-gap states did not exhibit any change and the E_F position still remained shifted after 8 h from white light irradiation stress (Fig. 4). Therefore, the extra in-gap states can be ascribed to V_O^{2+}. Because V_O^{2+} is the metastable donor, the creation of V_O^{2+} results in the E_F position to the vacuum level side.

The metastable peroxide defect ($(O\text{–}O)^{2-}$) can be another metastable donor created by light irradiation. Nahm *et al.* revealed that holes photo-excited by UV and visible light create a metastable peroxide defect $(O\text{–}O)^{2-}$ whose two electrons occupy CB and result in a shift of the E_F to the vacuum level side[14]. They calculated an energy barrier to be 0.97 eV from the metastable state ($(O\text{–}O)^{2-}$) to the initial state ($2O^{2-}$). Meux *et al.* reported that the recovery energy barriers from a peroxide defect to an initial state are in the range from 0.84 to 1.23 eV[15]. Robertson *et al.* revealed that oxygen interstitials, present to compensate hydrogen donors, allow metastable $(O\text{–}O)^{2-}$ state due to light irradiation. This can lead to persistent photoconductivity with an energy barrier for the transition from the meta-stable donor state to the ground state[80]. Therefore, extra in-gap states can be ascribed to not only V_O^{2+} but also $(O\text{–}O)^{2-}$.

Another possible origin can be the photo-desorption of oxygen-related species, which is proposed as a mechanism of device instability due to IS and NBIS. In this mechanism[6,8], first, oxygen adsorbed on the surface attracts electrons and induces upward band bending near the surface, O_2 (gas) + e^- = O_2^- (solid). Under light irradiation, holes made by photoexcitation promote the photo-desorption of oxygen-related species, O_2^- (solid) + h^+ = O_2 (gas), which negatively shifts the subthreshold voltage in a-IGZO TFTs. Applying this mechanism to our results reveals that light irradiation may induce the photo-desorption reaction to cancel band bending, leading to the shift of E_F position to the vacuum level side. The extra in-gap states may be attributed to states due to the photo-desorption of oxygen-related species.

Next, we discuss the origin of near-CBM states observed by SR-HSUPS in Fig. 5. Because the lineshape of the SR-HSUPS spectrum resembles that of the CFS-YS spectrum after light irradiation stress, the near-CBM states observed in the SR-HSUPS should be ascribed to metastable donor states (V_O^{2+} or $(O\text{–}O)^{2-}$) or electrons due to photodesorption of oxygen-related species. Because metastable donor states are created by the photoexcitation from occupied in-gap states to empty states, photon energy and photon flux of excitation light in SR-HSUPS are qualitatively high and intense enough to create metastable donor states, respectively. Photon energy differed between the measurement light of SR-HSUPS and light irradiation stress, but photon flux is dominant in creating metastable donor states. Creating metastable donors and causing photodesorption of oxygen-related species due to excitation light of SR-HSUPS result in the shift of the E_F position to the vacuum level side. As a result, VBM energy from E_F determined by SR-HSUPS is 0.4 eV larger than the VBM energy determined by CFS-YS in Sec. III A.

The intensity of near-CBM states observed through HAXPES at $E_B^V = 3.8$–5 eV is approximately 100 times stronger than those through CFS-YS after white light irradiation and SR-HSUPS. It is unclear why the intensity of near-CBM states obtained by HAXPES is the highest among PESs, but the results can agree with the suggestion that near-CBM states in HAXPES are metastable states created by high-energy photons[41] for the following two reasons. (i) Hard X-ray irradiation can generate many holes in occupied in-gap states, as in the case of UV irradiation. (ii) The energy region of the near-CBM states observed by HAXPES is the same as that by SR-HSUPS.

As another interpretation of near-CBM states, band-filling is considered. Here, the deconvoluted LEIPS spectrum is positioned by aligning the E_F position of the LEIPS and CFS-YS spectrum. Note that the CFS-YS spectrum is that for the fresh sample. Here, the difference in the work function between the CFS-YS and LEIPS spectrum is within the experimental error as follows. The work function of the LEIPS spectrum is determined to be 4.2 eV by the peak energy of the first derivative of the LEET spectrum in LEIPS. The work function of the CFS-YS spectrum is obtained to be 4.32 eV by the

Journal of Applied Physics ACCEPTED MANUSCRIPT
AIP Publishing
This is the author's peer reviewed, accepted manuscript. However, the online version of record will be different from this version once it has been copyedited and typeset.
PLEASE CITE THIS ARTICLE AS DOI: 10.1063/5.0185405

SECO of the HS-UPS spectrum just before the CFS-YS measurement for the fresh sample. Since the total energy error in the determination of the E_F from the metal substrate and the vacuum level from the a-IGZO film is ±0.1 eV for each measurement, the energy error of the VB placement with respect to the CB is ±0.15 eV. The E_F positions of the CFS-YS spectrum after white light irradiation stress, HAXPES, and SR-HSUPS spectra are located shallower than the CBM position ($E_B^V = 4.05$ eV) determined by LEIPS. Therefore, creating metastable donors and/or causing photo-desorption of oxygen-related species by intense light irradiation results in the shifts of E_F into the CB, and then the band-filling should occur in a part of the CB bottom.

Next, we comment on the advantages and disadvantages of PES techniques. In principle, the probing depth of CFS-YS, SR-HSUPS and HAXPES are almost the same, a few nm or more[48,57]. Therefore, the fact that near-VBM states are observed among HAXPES, SR-HSUPS and CFS-YS agrees with previous studies which revealed that the near-VBM states concentrate in the surface region[41].

From the viewpoint of photoionization cross-section, HAXPES and SR/HeI-UPS are complementary methods: UPS can strongly detect the PDOS of O and Zn states, and HAXPES can strongly detect the PDOS of In and Ga states. Referring to the VB, because most of VB is dominated by the PDOS of O states for most oxides, UPS can be an effective method for investigating the total DOS of the VB in oxides (Fig. 1). Referring to the near-VBM states, although the origin of near-VBM states is not identified, it is interesting that the lineshape and intensity of near-VBM states are similar among the CFS-YS, SR-HSUPS, and HAXPES spectra (Fig. 5). This phenomenon indicates that the PDOS of each atomic orbital may be comparable in near-VBM states. According to the calculated PDOS of V_O in the literature[83], the PDOS of O, Zn, and In states are comparable in V_O, which is consistent with our results. With more information on the PDOS of in-gap states becoming available by calculations, comparing PESs and calculations will deepen the understanding of the in-gap states.

We comment on sample damage caused by the measurement light of PESs and the dynamic range of detected DOS of occupied in-gap states. CFS-YS successfully determines the DOS of occupied in-gap states without sample damage using low-energy and low-flux photons compared to other methods. The dynamic range of detected DOS of occupied in-gap states is approximately six orders of magnitude in CFS-YS. Near-VBM and CBM states are observed in HAXPES and SR-HSUPS measurements. But near-CBM states are most likely not intrinsic states of undamaged a-IGZO and are derived from the intense light irradiation of SR in measurements. Creating large DOS of near-CBM states due to measurement lights limits dynamic range of detected DOS of occupied in-gap states by only two orders of magnitude in HAXPES. We emphasize that CFS-YS is a useful method to determine the DOS of occupied in-gap states of the samples that are sensitive to light irradiation. Future studies on the in-gap states of a-IGZO should refer to the intrinsic DOS obtained by CFS-YS. Also, in-gap states have been reported in other oxides[6,12,58–66], as in the case of a-IGZO. CFS-YS will widely contribute to understanding the electronic states of these materials.

From the perspective of device applications, it is notable that CFS-YS can directly observe the changes in in-gap states due to light irradiation stress by using low-energy and low-flux photons. Previous studies have suggested that the metastable donors (V_O^{2+}[1–3,6,9–13] or $(O–O)^{2-}$[12,14–17]) or photo-desorption of oxygen-related species[6,8] result in the instability issue of TFTs under IS and NBIS. In CFS-YS experiments in Fig. 4, the photon flux of light irradiation stress at $h\nu = 4.06$ eV is approximately the same as that of the light irradiation of IS[13] and NBIS[5] in the literature. The change in electronic states due to light irradiation stress observed by CFS-YS qualitatively agrees with the above instability mechanisms due to NBIS and IS. Also, Mativenga *et al.* proposed that the photo-degradation of TFTs mainly occurs within a few nm of the surface[1]. CFS-YS can detect the electronic states in that region. Furthermore, in the case of a-IGZO, Lee *et al.* suggested that the metastable donor results in persistent photoconductivity (PPC), which is the prolonged decay photoresponses with time constants $> 10^3$ s[88]. Extra in-gap states observed by CFS-YS may be related to PPC. CFS-YS experiments will directly elucidate PPC and instability mechanisms by investigating the relationship between changes in electronic states and device performances due to light irradiation. For example, to identify the origin of extra in-gap states, it is important to perform CFS-YS measurements after re-annealing the sample or irradiating it with a low-energy electron beam to recover the initial sample conditions as future efforts. It is also a good strategy to grow a crystalline phase of the film and try a local identification of the defects studied by scanning probe microscope techniques. Furthermore, TFTs based on other transparent oxide semiconductors[6,12,66] have faced on same instability issue due to IS and NBIS. Utilizing CFS-YS will widely contribute to the improvement of devices using transparent oxide semiconductors.

F. Optical absorption and simulation

In this section, we discuss how the DOS of occupied in-gap states should be deduced by using the optical absorption spectrum. Figure 6 (a) displays the optical absorption spectrum that is made by overlapping the results of PDS and ellipsometry. The Tauc plot determines the optical band gap to be 3.24 eV. This value is consistent with that of a sample with similar Hall mobility and concentration in the literature[77].

In the literature, the lineshape at $h\nu = 2.8$–3.0 eV is ascribed to the Urbach tail[23,35,83] and the DOS lineshape of occupied in-gap states is estimated by substituting E_u at $h\nu = 2.8$–3.0 eV for E_{0v}[23,35]. In this study, E_u is determined to be 0.11 eV by the PDS spectrum in log scale (Fig. 6(b)), corresponding to the value of literature[23,35,83]. By following previous works[23,35], the DOS lineshape is deduced by substituting E_u for E_{0v} (Fig. 5). But, the DOS lineshape estimated by E_u differs from that directly determined by other PES results (Fig. 5). We find that the DOS lineshape of occupied in-gap states cannot be estimated by substituting E_u for E_{0v} in the case of a-IGZO. Although we have no imformation of E_{0v} of

AIP Publishing
Journal of Applied Physics
ACCEPTED MANUSCRIPT
This is the author's peer reviewed, accepted manuscript. However, the online version of record will be different from this version once it has been copyedited and typeset.
PLEASE CITE THIS ARTICLE AS DOI: 10.1063/5.0185405

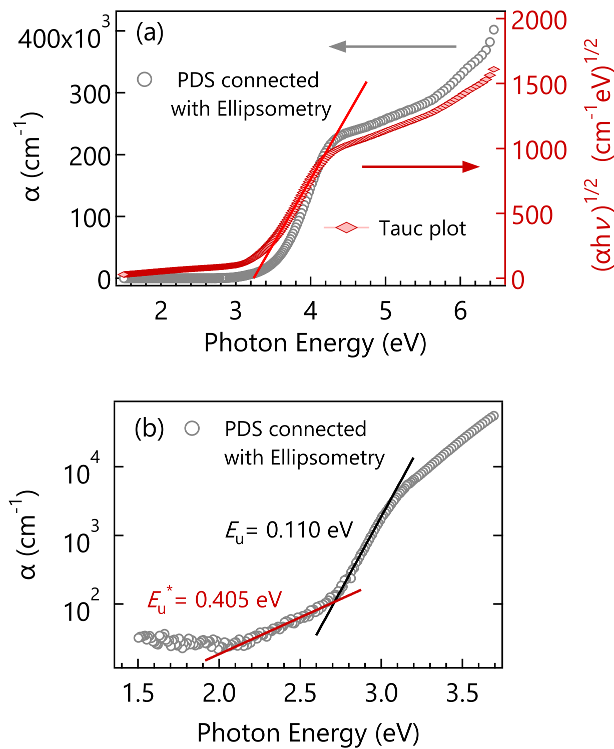

FIG. 6. (a) Absorption spectrum constructed from ellipsometry and PDS results (empty grey circle) in the left axis. The value of $\sqrt{\alpha h\nu}$ was plotted at the right axis as the Tauc plot (solid red diamond). (b) PDS spectrum in the low hν region on the semi-log scale.

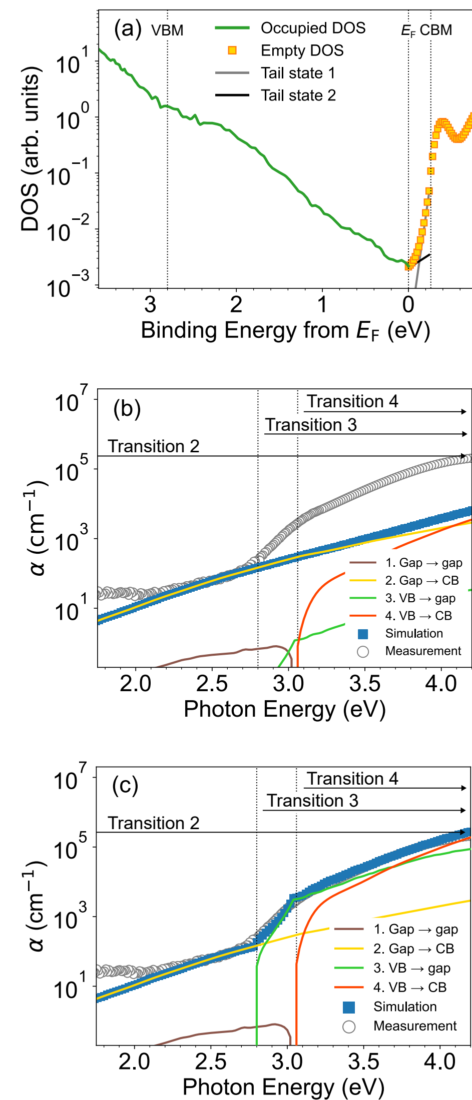

FIG. 7. (a) Density of states (DOS) used to calculate the α spectrum. E_F for the fresh sample was set at 0.0 eV. The occupied DOS was determined through CFS-YS after white light irradiation stress in Fig. 5. The CB was determined from the deconvoluted LEIPS spectrum. Empty in-gap states were assumed to consist of two tail states. The slope parameters are 0.04 and 0.44 eV. (b) Comparison between the PDS and the simulation by calculation of multiplying joint DOS and photon energy using measured DOS in (a). This calculation was under the assumption that $|M_{fi}|^2$ was constant. Transition 1–4 indicates the transition from occupied in-gap states to empty in-gap states, from the VB to empty in-gap states, from occupied in-gap states to the CB, and from the VB to CB. (c) The simulation was performed under the assumption that the transition probability, $|M_{fi}|^2$, was a different constant for each transition 1–4 in (b).

the CFS-YS spectrum in this sample, note that the DOS lineshape estimated by E_u can be directly compared with the DOS lineshapes determined by PESs since α is expressed by joint DOS (Eq. (1)).

We have another option to deduce the DOS curve of occupied in-gap states by using the lineshape at h$\nu = 2.2$–2.7 eV in the PDS spectrum. In this article, the PDS spectrum of this region is called "exponential tail" to distinguish it from the Urbach tail. Note that the region at h$\nu < 2.1$ eV is the background. The slope of this exponential tail is 0.405 eV. In this study, this slope is denoted as E_u^* to distinguish it from the E_u. The DOS distribution of occupied in-gap states is estimated by substituting E_u^* for E_{0v} in Fig. 5. We reveal that it is consistent with the DOS curves directly determined by SR-HSUPS and CFS-YS. Note that CFS-YS indicates the measurement after white light irradiation stress. The a-IGZO film is expected to be not free from photo-degradation in the PDS measurement because the photon flux of excitation light in PDS was roughly estimated to be 10^{15} to 10^{16} cm^{-2}s^{-1}.

To discuss the validity of deducing the DOS lineshape of occupied in-gap states by assuming E_u or E_u^* as E_{0v}, the PDS spectrum was simulated according to Eq. (1). D_i was obtained by the CFS-YS spectrum after white light irradiation stress shown as Fig. 7(a). D_f was obtained by the deconvoluted LEIPS spectrum. D_i and D_f were normalized by comparison with the theoretical calculated DOS[39]. In the calculation of Eq. (1), the E_F was assumed to be that for the fresh sample in the Fig. 4, and D_i under E_F was excluded because the transition from the extra in-gap states under E_F to the empty states did not affect the PDS spectral analysis above 2 eV. Empty in-gap states were assumed to be two tail states, referring to the literature[17]. The slope parameters of added tail states were 0.04 and 0.44 eV, and D_f was connected with D_i at E_F. In Fig.

AIP Publishing Journal of Applied Physics ACCEPTED MANUSCRIPT
This is the author's peer reviewed, accepted manuscript. However, the online version of record will be different from this version once it has been copyedited and typeset.
PLEASE CITE THIS ARTICLE AS DOI: 10.1063/5.0185405

7(a), CBM was assumed to be at $E_B^F = -0.26$ eV. VBM was assumed to be at $E_B^F = 2.8$ eV, where the slopes of the DOS curve were changed in the log scale.

Figure 7(b) presents a comparison of the measurement and a simulation. The simulation spectrum calculated by convolution of D_i and D_f can not reproduce the lineshape of the measurement. The simulation spectrum is divided into four transitions from occupied in-gap states to empty in-gap states (transition 1), from occupied in-gap states to the CB (transition 2), from the VB to empty in-gap states (transition 3), and from the VB to CB (transition 4). The intensity of transition 2 is considerably higher than transitions 3 and 4, which is unnatural. This result should be attributed to $|M_{fi}|^2$ effect. $|M_{fi}|^2$ must be different among transitions 1–4 because the wave functions of the VB top, CB bottom, and in-gap states are different. Actually, in the case of a-Si, $|M_{fi}|^2$ depends on the excitation photon energy[70].

The simulation was performed again, assuming that $|M_{fi}|^2$ for transitions 1–4 was a different constant as a rough approximation, which is shown in Fig. 7(c). Transitions 3 and 4 were multiplied by 2586 and 58, respectively. The simulation spectrum reproduces the measurement at $h\nu = 2.2$–4 eV. In the region at $h\nu = 2.2$–2.8 eV and $h\nu = 2.8$–3 eV, transitions 2 and 3 are the primary components, respectively. This indicates that (i) the lineshape of the Urbach tail ($h\nu = 2.8$–3.0 eV) does not reflect the DOS lineshape of occupied in-gap states (transition 2) but rather that of empty in-gap states (transition 3), and (ii) the exponential tail at $h\nu = 2.2$–2.7 eV is ascribed to transition 2. Thus, the DOS lineshape deduced by E_u^* more correctly reflects that of occupied in-gap states than that deduced by E_u.

We discuss that the slope of the Urbach tail at 2.8–3.0 eV coincides with the slope of the DOS of CFS-YS for the fresh sample at $E_B^V = 4.5$–5.5 eV in Fig. 5. It is a coincidence because occupied DOS at $E_B^V = 4.5$–5.5 eV mainly results in the absorption spectrum at $h\nu = 0.2$–1.5 eV.

Note that this absorption simulation includes the following possible errors. (i) Because of the difference of photon energy and photon flux in each measurement, the D_i determined by CFS-YS after white light irradiation stress may not completely reflect the D_i in PDS measurement. (ii) The probing depth may differ: CFS-YS and LEIPS mainly probe electronic states within several nm from the surface, and PDS observes absorption in the bulk. (iii) The energy error of the occupied DOS placement with respect to the empty DOS is ± 0.15 eV. But, this energy error does not significantly affect the conclusion that the exponential tail at $h\nu = 2.2$–2.7 eV in the PDS spectrum reflects the DOS lineshape of occupied in-gap states because the slope of transition 2 does not change much at $h\nu > 2$ eV.

We attempted to determine the DOS of empty in-gap states. In principle, deconvolution of the absorption spectrum and the DOS can determine it because PES methods have already determined the DOS except empty in-gap states. However, as shown in Fig. 7(b)(c), the $|M_{fi}|^2$ for each transition differs considerably, the DOS of empty in-gap states could not be determined.

IV. CONCLUSION

We examined the electronic states of the a-IGZO thin film using several spectroscopic techniques to provide the landscape of the reliable DOS of the VB, CB, and occupied in-gap states.

The CB was determined by LEIPS, which has a high energy resolution and low sample damage. We can obtain the DOS curve consistent with the calculated DOS obtained by first-principles calculation. We reveal that LEIPS is useful for obtaining the DOS of the CB of a-IGZO.

The DOS of occupied in-gap states is accurately determined without sample damage through CFS-YS measurement. We reveal that the excitation light of SR in SR-(HS)UPS and HAXPES measurements causes the sample damage: the creation of extra in-gap states and the shift of E_F into the CB. Near-CBM states reported in previous HAXPES works[41,42] are most likely not intrinsic electronic states of undamaged a-IGZO. We demonstrate that CFS-YS can become the standard method for directly and accurately obtaining the DOS of the samples that are sensitive to irradiation light, such as a-IGZO. In-gap states of a-IGZO should be discussed based on the intrinsic DOS obtained by CFS-YS.

CFS-YS directly observes the creation of extra in-gap states around E_F and the shift of E_F into the CB with light irradiation stress. These electronic state changes remain even 8 h after the light radiation stress. Judging from these facts, extra in-gap states (near-CBM states) should derive from metastable donors (V_O^{2+} and/or $(O\text{–}O)^{2-}$), states due to photo-desorption of oxygen-related species, or states due to electrons accumulated in the CB bottom (band-filling effect). These states should be related to persistent photocurrent and device instabilities due to NBIS and IS. These phenomena are widely reported in devices made by transparent amorphous oxide semiconductors, and utilizing CFS-YS will contribute to the improvement of devices using transparent amorphous oxide semiconductors.

The PDS spectrum is interpreted by the simulation based on measured DOS and indicates that (i) the Urbach tail (the PDS spectrum at $h\nu = 2.8$–3.0 eV) should reflect the transition of empty in-gap states rather than that of occupied in-gap states, and (ii) the PDS lineshape in the energy region below the region of the Urbach tail is derived from the transition of occupied in-gap states and roughly reflects the DOS lineshape of occupied in-gap states.

ACKNOWLEDGMENTS

This work was supported by a Japan Society for the Promotion of Science (JSPS) KAKENHI Grant-in-Aid for Scientific Research (B) (No. 16H04222, 20H02810) and by Japan Science and Technology Agency (JST), the establishment of university fellowships towards the creation of science technology innovation (No. JPMJFS2107). A part of this work was conducted at the BL7U (SAMRAI) of UVSOR Synchrotron Facility, Institute for Molecular Science (IMS program 22IMS6855). The synchrotron radiation experiments in

ACCEPTED MANUSCRIPT
Journal of Applied Physics
AIP Publishing
This is the author's peer reviewed, accepted manuscript. However, the online version of record will be different from this version once it has been copyedited and typeset.
PLEASE CITE THIS ARTICLE AS DOI: 10.1063/5.0185405

hard X-ray region were performed at the BL46XU of SPring-8 with the approval of the Japan Synchrotron Radiation Research Institute (JASRI) (Proposal No. 2020A1824). R.N. would also like to thank the Frontier Science Program for Graduate Students of Chiba University for its financial support. M.A.-J. acknowledges the Department for Energy Security and Net Zero (Project ID: NEXTCCUS), University College London's Research, Innovation and Global Engagement, University of Sydney-University College London Partnership Collaboration Awards, and Cornell-UCL Global Strategic Collaboration Awards for their financial support. M.A.-J. acknowledges the ACT program (Accelerating CCS Technologies, Horizon2020 Project No. 691712) for the financial support of the NEXTCCUS project (project ID: 327327). M.A.-J. acknowledges the Royal Society (RGS\R1\211068) and Cambridge Materials Limited for their funding and technical support. S. D. S. acknowledges the Royal Society (UF150033) for funding.

CONFLICT OF INTEREST

The authors have no conflicts to disclose.

DATA AVAILABILITY

The data that support the findings of this study are available from the corresponding author upon reasonable request.

[1]M. Mativenga, F. Haque, M. M. Billah, and J. G. Um, Sci. Rep. **11**, 1–12 (2021).
[2]H. Oh, S. M. Yoon, M. K. Ryu, C. S. Hwang, S. Yang, and S. H. K. Park, Appl. Phys. Lett. **97**, 183502 (2010).
[3]M. P. Hung, D. Wang, J. Jiang, and M. Furuta, ECS Solid State Lett. **3**, Q13 (2014).
[4]K. M. Yu, S. H. Jeong, B. S. Bae, and E. J. Yun, J. Korean Phys. Soc. **61**, 852–857 (2012).
[5]M. M. Billah, M. D. H. Chowdhury, M. Mativenga, J. G. Um, R. K. Mruthyunjaya, G. N. Heiler, T. J. Tredwell, and J. Jang, IEEE Electron Device Lett. **37**, 735–738 (2016).
[6]J. K. Jeong, J. Mater. Res. **28**, 2071–2084 (2013).
[7]K. Nomura, T. Kamiya, and H. Hosono, Appl. Phys. Lett. **99**, 053505 (2011).
[8]S. Y. Huang, T. C. Chang, M. C. Chen, T. C. Chen, F. Y. Jian, Y. C. Chen, H. C. Huang, and D. S. Gan, Surf. Coat. Technol. **231**, 117–121 (2013).
[9]S. Lee, A. Nathan, S. Jeon, and J. Robertson, Sci. Rep. **5**, 1–10 (2015).
[10]K. H. Ji, J. I. Kim, H. Y. Jung, S. Y. Park, R. Choi, U. K. Kim, C. S. Hwang, D. Lee, H. Hwang, and J. K. Jeong, Appl. Phys. Lett. **98**, 1–4 (2011).
[11]Y. Seung Rim, W. Jeong, B. Du Ahn, and H. Jae Kim, Appl. Phys. Lett. **102**, 143503 (2013).
[12]J. Jang, D. G. Kim, D. M. Kim, S. J. Choi, J. H. Lim, J. H. Lee, Y. S. Kim, B. D. Ahn, and D. H. Kim, Appl. Phys. Lett. **105**, 152108 (2014).
[13]M. D. H. Chowdhury, P. Migliorato, and J. Jang, Appl. Phys. Lett. **97**, 173506 (2010).
[14]H. H. Nahm, Y. S. Kim, and D. H. Kim, Phys. Status Solidi B **249**, 1277–1281 (2012).
[15]A. de Jamblinne de Meux, G. Pourtois, J. Genoe, and P. Heremans, J. Appl. Phys. **123**, 161513 (2017).
[16]A. de Jamblinne de Meux, G. Pourtois, J. Genoe, and P. Heremans, Phys. Rev. Appl. **9**, 054039 (2018).
[17]S. Choi, J. Park, S. H. Hwang, C. Kim, Y. S. Kim, S. Oh, J. H. Baeck, J. U. Bae, J. Noh, S. W. Lee, K. S. Park, J. J. Kim, S. Y. Yoon, H. I. Kwon, and D. H. Kim, Adv. Electron. Mater. **8**, 2101062 (2022).
[18]T. Kamiya, K. Nomura, and H. Hosono, Sci. Technol. Adv. Mater. **11**, 044305 (2010).
[19]K. Ide, K. Nomura, H. Hosono, and T. Kamiya, Phys. Status Solidi A **216**, 1–28 (2019).
[20]H. Bae, H. Choi, S. Jun, C. Jo, Y. H. Kim, J. S. Hwang, J. Ahn, S. Oh, J.-U. Bae, S.-J. Choi, D. H. Kim, and D. M. Kim, IEEE Electron Device Lett. **34**, 1524–1526 (2013).
[21]S. Lee, S. Park, S. Kim, Y. Jeon, K. Jeon, J.-H. Park, J. Park, I. Song, C. J. Kim, Y. Park, D. M. Kim, and D. H. Kim, IEEE Electron Device Lett. **31**, 231–233 (2010).
[22]K. Abe, A. Sato, K. Takahashi, H. Kumomi, T. Kamiya, and H. Hosono, Thin Solid Films **559**, 40–43 (2014).
[23]E. K. H. Yu, S. Jun, D. H. Kim, and J. Kanicki, J. Appl. Phys. **116** (2014).
[24]Y. Kim, M. Bae, W. Kim, D. Kong, H. K. Jung, H. Kim, S. Kim, D. M. Kim, and D. H. Kim, IEEE Trans. Electron Devices **59**, 2689–2698 (2012).
[25]J. T. Jang, J. Park, B. D. Ahn, D. M. Kim, S. J. Choi, H. S. Kim, and D. H. Kim, ACS Appl. Mater. Interfaces **7**, 15570–15577 (2015).
[26]S. Choi, J.-Y. Kim, J. Rhee, H. Kang, S. Park, D. M. Kim, S.-J. Choi, and D. H. Kim, IEEE Electron Device Lett. **40**, 574 (2019).
[27]M. C. Nguyen, A. H. T. Nguyen, H. Ji, J. Cheon, J. H. Kim, K. M. Yu, S. Y. Cho, S. W. Kim, and R. Choi, IEEE Trans. Electron Devices **65**, 3786–3790 (2018).
[28]H. Im, H. Song, J. Park, Y. Hong, J. Ha, S.-B. Ji, J. Jeong, and Y. Hong, IEEE Trans. on Electron Devices **64**, 1683–1688 (2017).
[29]H. Lee, J. Kim, S. Choi, S. K. Kim, J. Kim, J. Park, S.-J. Choi, D. H. Kim, and D. M. Kim, IEEE Electron Device Lett. **38**, 199–202 (2017).
[30]H. Bae, H. Seo, S. Jun, H. Choi, J. Ahn, J. Hwang, J. Lee, S. Oh, J.-U. Bae, S.-J. Choi, D. H. Kim, and D. M. Kim, IEEE Trans. on Electron Devices **61**, 3566–3569 (2014).
[31]S. Jun, C. Jo, H. Bae, H. Choi, D. H. Kim, and D. M. Kim, IEEE Electron Device Lett. **34**, 641–643 (2013).
[32]W. Chen, W. Wu, L. Zhou, M. Xu, L. Wang, H. Ning, and J. Peng, Materials **11**, 416 (2018).
[33]L. Qiang and R. H. Yao, J. Disp. Technol. **11**, 325–329 (2015).
[34]Y. Kim, S. Kim, W. Kim, M. Bae, H. K. Jeong, D. Kong, S. Choi, D. M. Kim, and D. H. Kim, IEEE Trans. Electron Devices **59**, 2699–2706 (2012).
[35]T.-C. Fung, C.-S. Chuang, C. Chen, K. Abe, R. Cottle, M. Townsend, H. Kumomi, and J. Kanicki, J. Appl. Phys. **106**, 084511 (2009).
[36]F. Urbach, Phys. Rev. **92**, 1324–1324 (1953).
[37]J. D. Joannopoulos and G. Lucovsky, *The physics of hydrogenated amorphous silicon II: Electronic and Vibrational Properties* (Springer Science & Business Media, 2008).
[38]K. Winer and L. Ley, Phys. Rev. B **36**, 6072–6078 (1987).
[39]Z. Zhang, Y. Guo, and J. Robertson, J. Appl. Phys. **128**, 215704 (2020).
[40]J. J. Yeh and I. Lindau, At. Data Nucl. Data Tables **32**, 1–155 (1985).
[41]K. Nomura, T. Kamiya, E. Ikenaga, H. Yanagi, K. Kobayashi, and H. Hosono, J. Appl. Phys. **109**, 073726 (2011).
[42]K. Nomura, T. Kamiya, H. Yanagi, E. Ikenaga, K. Yang, K. Kobayashi, M. Hirano, and H. Hosono, Appl. Phys. Lett. **92**, 202117 (2008).
[43]N. Oka, T. Aoi, R. Hayashi, H. Kumomi, and Y. Shigesato, Appl. Phys. Express **5**, 075802 (2012).
[44]S. Sallis, K. T. Butler, N. F. Quackenbush, D. S. Williams, M. Junda, D. A. Fischer, J. C. Woicik, N. J. Podraza, J. White, B. E., A. Walsh, and L. F. J. Piper, Appl. Phys. Lett. **104**, 232108 (2014).
[45]S. Sallis, N. F. Quackenbush, D. S. Williams, M. Senger, J. C. Woicik, B. E. White, and L. F. Piper, Phys. Status Solidi A **212**, 1471–1475 (2015).
[46]H. Tang, K. Ide, H. Hiramatsu, S. Ueda, N. Ohashi, H. Kumomi, H. Hosono, and T. Kamiya, Thin Solid Films **614**, 73–78 (2016).
[47]K. Lee, K. Nomura, H. Yanagi, T. Kamiya, E. Ikenaga, T. Sugiyama, K. Kobayashi, and H. Hosono, J. Appl. Phys. **112**, 033713 (2012).
[48]S. Hüfner, *Photoelectron spectroscopy: principles and applications* (Springer Science & Business Media, 2013).
[49]R. Nakazawa, A. Matsuzaki, K. Shimizu, E. Kawashima, M. Abdi-Jalebi, S. D. Stranks, Y. Tanaka, H. Tokairin, and H. Ishii, Appl. Phys. Express **14**, 071004 (2021).
[50]M. Sebastiani, L. Di Gaspare, G. Capellini, C. Bittencourt, and F. Evangelisti, Phys. Rev. Lett. **75**, 3352–3355 (1995).
[51]L. Korte, A. Laades, and M. Schmidt, J. Non-Cryst. Solids **352**, 1217–1220 (2006).
[52]L. Korte and M. Schmidt, J. Non-Cryst. Solids **354**, 2138–2143 (2008).

AIP Publishing Journal of Applied Physics ACCEPTED MANUSCRIPT
This is the author's peer reviewed, accepted manuscript. However, the online version of record will be different from this version once it has been copyedited and typeset.
PLEASE CITE THIS ARTICLE AS DOI: 10.1063/5.0185405

[53]D. Menzel, A. Tejada, A. Al-Ashouri, I. Levine, J. A. Guerra, B. Rech, S. Albrecht, and L. Korte, ACS Appl. Mater. Interfaces **13**, 43540–43553 (2021).
[54]I. Levine, K. Shimizu, A. Lomuscio, M. Kulbak, C. Rehermann, A. Zohar, M. Abdi-Jalebi, B. Zhao, S. Siebentritt, F. Zu, N. Koch, A. Kahn, G. Hodes, R. H. Friend, H. Ishii, and D. Cahen, J. Phys. Chem. C **125**, 5217–5225 (2021).
[55]D. Menzel, A. Al-Ashouri, A. Tejada, I. Levine, J. A. Guerra, B. Rech, S. Albrecht, and L. Korte, Adv. Energy Mater. **12**, 2201109 (2022).
[56]K. Shimizu, H. Tokairin, R. Nakazawa, I. Nakamura, S. Yasuno, K. Ikegami, Y. Yamaguchi, Y. Tanaka, and H. Ishii, Appl. Phys. Express **15**, 094002 (2022).
[57]Y. Ozawa, Y. Nakayama, S. Machida, H. Kinjo, and H. Ishii, J. Electron Spectrosc. Relat. Phenom. **197**, 17 (2014).
[58]X. Shao, J.-F. Jerratsch, N. Nilius, and H.-J. Freund, Phys. Chem. Chem. Phys. **13**, 12646 (2011).
[59]T. Götsch, E. Bertel, A. Menzel, M. Stöger-Pollach, and S. Penner, Phys. Rev. Mater. **2**, 035801 (2018).
[60]T. Nikolay, L. Larina, O. Shevaleevskiy, and B. T. Ahn, Energy Environ. Sci. **4**, 1480 (2011).
[61]Sakar, Prakash, and Do, Catalysts **9**, 680 (2019).
[62]D.-p. Bui, M.-t. Pham, H.-h. Tran, T.-d. Nguyen, T. M. Cao, and V. V. Pham, ACS Omega **6**, 27379–27386 (2021).
[63]J. Li, R. Lazzari, S. Chenot, and J. Jupille, Phys. Rev. B **97**, 041403 (2018).
[64]L. Grządziel, M. Krzywiecki, A. Szwajca, A. Sarfraz, G. Genchev, and A. Erbe, J. Phys. D: Appl. Phys. **51**, 315301 (2018).
[65]M. J. Wahila, Z. W. Lebens-Higgins, K. T. Butler, D. Fritsch, R. E. Treharne, R. G. Palgrave, J. C. Woicik, B. J. Morgan, A. Walsh, and L. F. J. Piper, APL Mater. **7**, 022509 (2018).
[66]Z. Yang, T. Meng, Q. Zhang, and H. P. D. Shieh, IEEE Electron Device Lett. **37**, 437–440 (2016).
[67]M.-H. Kim, Y.-A. Lee, J. Kim, J. Park, S. Ahn, K.-J. Jeon, J. W. Kim, D.-K. Choi, and H. Seo, ACS Nano **9**, 9964–9973 (2015).
[68]H. Yoshida, Chem. Phys. Lett. **539-540**, 180–185 (2012).
[69]H. Yoshida, J. Electron Spectrosc. Relat. Phenom. **204**, 116 (2015).
[70]W. B. Jackson, S. M. Kelso, C. C. Tsai, J. W. Allen, and S.-J. Oh, Phys. Rev. B **31**, 5187–5198 (1985).
[71]S.-I. Kimura, T. Ito, M. Sakai, E. Nakamura, N. Kondo, T. Horigome, K. Hayashi, M. Hosaka, M. Katoh, T. Goto, T. Ejima, and K. Soda, Rev. Sci. Instrum. **81**, 053104 (2010).
[72]H. Ota, E. Salehi, M. Fujimoto, K. Hayashi, T. Horigome, H. Iwayama, M. Katoh, N. Kondo, S. Makita, F. Matsui, H. Matsuda, T. Mizukawa, A. Minakuchi, E. Nakamura, M. Nagasaka, Y. Okano, T. Ohigashi, M. Sakai, K. Sugita, K. Tanaka, Y. Taira, F. Teshima, J.-i. Yamazaki, T. Yano, H. Yuzawa, and S. Kera, J. Phys.: Conf. Ser. **2380**, 012003 (2022).
[73]S. Yasuno, H. Oji, T. Koganezawa, and T. Watanabe, AIP Conf. Proc. **1741**, 030020 (2016).
[74]H. Yoshida, Rev. Sci. Instrum. **85**, 016101 (2014).
[75]P. A. Jansson, *Deconvolution of images and spectra* (Courier Corporation, 2014) p. 114–116.
[76]M. Abdi-Jalebi, M. I. Dar, S. P. Senanayak, A. Sadhanala, Z. Andaji-Garmaroudi, L. M. Pazos-Outón, J. M. Richter, A. J. Pearson, H. Sirringhaus, M. Grätzel, and R. H. Friend, Sci. Adv. **5**, 1–10 (2019).
[77]H. Tang, Y. Kishida, K. Ide, Y. Toda, H. Hiramatsu, S. Matsuishi, S. Ueda, N. Ohashi, H. Kumomi, H. Hosono, and T. Kamiya, ECS J. Solid State Sci. Technol. **6**, P365–P372 (2017).
[78]A. Mirzehmet, T. Ohtsuka, S. A. Abd. Rahman, T. Yuyama, P. Krüger, and H. Yoshida, Adv. Mater. **33**, 2004981 (2021).
[79]W. Körner, D. F. Urban, and C. Elsässer, J. Appl. Phys. **114**, 163704 (2013).
[80]J. Robertson and Y. Guo, Appl. Phys. Lett. **104**, 162102 (2014).
[81]J. Kim, J. Bang, N. Nakamura, and H. Hosono, APL Mater. **7**, 022501 (2018).
[82]C. Kim, Y.-H. Kim, Y.-Y. Noh, S.-J. Hong, and M. J. Lee, Adv. Electron. Mater. **4**, 1700440 (2018).
[83]T. Kamiya, K. Nomura, M. Hirano, and H. Hosono, Phys. Status Solidi C **5**, 3098–3100 (2008).
[84]J. Bang, S. Matsuishi, and H. Hosono, Appl. Phys. Lett. **110**, 232105 (2017).
[85]H. Li, Y. Guo, and J. Robertson, Phys. Rev. Mater. **2**, 074601 (2018).
[86]B. Ryu, H. K. Noh, E. A. Choi, and K. J. Chang, Appl. Phys. Lett. **97**, 22108 (2010).
[87]H.-K. Noh, K. J. Chang, B. Ryu, and W.-J. Lee, Phys. Rev. B **84**, 115205 (2011).
[88]D. H. Lee, K. I. Kawamura, K. Nomura, T. Kamiya, and H. Hosono, Electrochem. Solid-State Lett. **13**, 324–327 (2010).